Tr. J. of Physics
23 (1999) , 125 – 157.

Electron Liquid Beyond the Random Phase Approximation

Mehmet TOMAK*
Department of Physics, Middle East Technical University
Ankara - 06531, TURKEY
Ceyhun BULUTAY†
Department of Electrical and Electronics Engineering
Middle East Technical University
Ankara - 06531, TURKEY

Received ...

Abstract

A deeper understanding of low-dimensional and small-scale electronic systems requires an accurate characterization of the many-electron effects. Based on the electron liquid (EL) model, these many-body effects in the three-dimensional (3D) and two-dimensional (2D) electronic systems are dealt going beyond the random phase approximation within the zero-temperature framework. The dielectric formulation of the many-body problem is recapitulated and the longitudinal dielectric function of the EL is obtained using the self-consistent local-field correction scheme, known as STLS, under a general spin-valley degeneracy. Extensive explicit expressions are provided for the use of other researchers. The performance of this formalism is compared in both 3D and 2D by the quantum Monte Carlo data and the pseudopotential approach introduced by Pines and co-workers. STLS is observed to be a highly satisfactory technique, with some reservations on the long-wavelength behaviour. Ground-state energy, correlation energy and the isothermal compressibility of the 2D EL are computed using a variety of approaches. Negative compressibility and overscreening are discussed in the light of the recent experiments.

1. Introduction

The electron liquid (EL) is a standard model system of many-body quantum mechanics [1, 2]. From the practical standpoint, the EL serves for the characterization of the conduction band electrons in metals and mobile carriers in doped semiconductors, especially with low-dimensions, such as heterojunctions, quantum wells, and to some extend quantum wires. The model considers interacting dynamic electrons over a homogeneous

*e-mail: mehmet-tomak@metu.edu.tr
†e-mail: ceyhun-bulutay@metu.edu.tr

positive background representing the ions and at the same time enabling the charge neutrality of the system. The background is taken to be rigid, and hence, nonpolarizable. This model is also named as the electron *gas* in part of the literature, but we prefer the word *liquid* as the correlations among the electrons are quite significant and towards low densities short-range order exists as in classical liquids. Further supports are given in the following text, within the discussion of the ground-state energy. As the quantum labels for the constituent electrons of the EL, we use the spin z-projection (σ), the wave vector ($\vec{k}$) and a valley index (ν) to account for the common case of energetically-degenerate valleys. The electrons are assumed to have an isotropic effective mass, m^* and the dielectric polarization of the *bound* electrons are incorporated by a background dielectric constant, κ. The shortcomings of the EL model in representing the real systems are mainly the lack of ionic lattice and disorder effects. The latter is to some extend remedied by introducing a phenomological imaginary part to the Lindhard function [3, 4]. As for the ionic lattice, the model can be extended to include the Fröhlich electron-phonon coupling [5]. However, we do not incorporate these extensions into our analysis. All throughout this work we work in zero-temperature, where the non-interacting Fermi occupation function is of the step form.

The long-range Coulomb interaction among the electrons renders impossible, the decoupling of individual electronic motions, and therefore, the EL remained to be the workhorse of many-body physics for the past four decades. Among the many alternatives, the dielectric formulation [6] of the many-body problem has proven to be logical, simple and yet quite accurate. The purpose of the present paper is twofold: guiding potential researchers by providing a self-contained account of the dielectric formulation of the EL, and presenting new results and assessments beyond the widely-used random phase approximation. Both the three and two-dimensional ELs are considered.

The electronic properties such as transport and screening in electronic devices are characterized by the *longitudinal* dielectric function whereas the optoelectronic properties are determined by the *transverse* dielectric function. In the following section we first establish this division by introducing the longitudinal and transverse dielectric functions starting from Maxwell's equations with a homogeneous medium in mind. However, in the remaining part of this work, the term "dielectric function" refers to the *longitudinal* one, which plays an utmost role in many physical quantities like carrier lifetime, mobility, ground-state energy, isothermal compressibility etc. In the plan of the paper, we then introduce the density response function based on the linear response formalism. Following this, we show the connection of the dielectric function with the diagrammatic quantity, the polarization insertion. The widely-used random phase approximation (RPA) is then readily obtained. Improvements of RPA using dynamic and static local-field correction are introduced and the self-consistent scheme, the so-called STLS technique that we employ, is reached. The relations between the static form factor and the dielectric function are given. We provide a comprehensive list of explicit expressions for both three-dimensional (3D) and two-dimensional (2D) ELs, again to aid potential researchers. As for the results, we first assess different treatments, including the available quantum Monte Carlo data, and the polarization potential theory developed by Pines and co-workers on the structure-

related quantities both in 3D and 2D. We compute the correlation energy, compressibility of the 2D EL within the STLS formalism and compare with other techniques. Interesting results such as negative electronic compressibility and overscreening are discussed and supplemented with recent experimental findings.

In this paper we present our results that were not published elsewhere. However, for reference purposes, we refer to Ref. [7] for the extension of this work to the quasi-2D EL in heterojunctions, furthermore, in Ref. [8], we investigate the effect of spin-valley degeneracy on the screening of charged impurity centers in 2D and 3D ELs.

2. The Dielectric Function

2.1. Basics

To probe any electronic response of a specific medium, we need to apply an excitation. For this purpose we assume an applied external charge density, $\varrho_{ext}(\vec{r},t)$ and its associated motion giving rise to the current density $\vec{j}_{ext}(\vec{r},t)$. In particular, we choose the excitation to be of a travelling-wave type with spatial variation characterized by wave number q and temporal variation by the angular frequency ω, so that,

$$\varrho_{ext}(\vec{r},t) = \rho_{ext}(\vec{q},\omega)\, \mathrm{e}^{i\vec{q}\cdot\vec{r}}\, \mathrm{e}^{-i\omega t}, \tag{1}$$

$$\vec{j}_{ext}(\vec{r},t) = \vec{J}_{ext}(\vec{q},\omega)\, \mathrm{e}^{i\vec{q}\cdot\vec{r}}\, \mathrm{e}^{-i\omega t}. \tag{2}$$

Note that, any arbitrary function of $(\vec{r},t)$ can be synthesized using the particular forms in Eqs. (1),(2) by means of the Fourier transform. Throughout this work, we assume a homogeneous medium. We must also mention that, we have independent control on the variables $\vec{q}$ and ω separately, that is to say, they are not related. So, we probe the electric response of the medium under an excitation with an arbitrary $(\vec{q},\omega)$ pair.

The charge and current densities are not independent but constrained by the continuity equation as

$$\nabla_{\vec{r}} \cdot \vec{j}_{ext}(\vec{r},t) = -\frac{\partial \varrho_{ext}(\vec{r},t)}{\partial t}, \tag{3}$$

which becomes in $(\vec{q},\omega)$ space

$$i\vec{q}\cdot\vec{J}_{ext}(\vec{q},\omega) = i\omega\rho_{ext}(\vec{q},\omega). \tag{4}$$

As a response to these excitations an electromagnetic field will be generated in the medium governed by Maxwell's equations which are listed below in cgs unit system

$$i\vec{q}\times\vec{B}(\vec{q},\omega) = -\frac{i\omega}{c}\vec{D}(\vec{q},\omega) + \frac{4\pi}{c}\vec{J}_{ext}(\vec{q},\omega), \tag{5}$$

$$i\vec{q}\times\vec{E}(\vec{q},\omega) = \frac{i\omega}{c}\vec{B}(\vec{q},\omega), \tag{6}$$

$$i\vec{q}\cdot\vec{D}(\vec{q},\omega) = 4\pi\rho_{ext}(\vec{q},\omega), \tag{7}$$

$$i\vec{q}\cdot\vec{B}(\vec{q},\omega)=0. \tag{8}$$

The dielectric function (DF) of a medium which is our primary quantity of interest is in general a tensor that relates the total electric field $\vec{E}$ to the displacement field $\vec{D}$ in that medium. If this relation is taken to be a linear one, it becomes

$$\vec{D}(\vec{q},\omega)=\overline{\overline{\epsilon}}\,(\vec{q},\omega)\,\vec{E}(\vec{q},\omega). \tag{9}$$

Obviously, this restricts our treatment to low electric field values. For example, in three-dimensional quantum Monte Carlo simulations, it has been observed that electric fields upto 2.0×10^8 V/cm, insure the linearity of the response [9]. It needs to be mentioned that, the dielectric constant was initially introduced to describe the reduction of the external field by the medium [10]. The classical texts on macroscopic electromagnetics (such as Ref. [11]) consider the dielectric constant concept to be applicable to dielectrics, that is to say, a medium having only bound charges that can, to some extend, polarize under an excitation. Here, we apply the dielectric constant concept (which now becomes a function of $\vec{q}$ and ω) to a medium made up of unbound electrons, called the *electron liquid*. To have an order of magnitude feeling, an appropriate length-scale for characterizing the size of the so-called nonlocality radius can be the Fermi wavelength, λ_F. In a medium with $n_{3D}=10^{18}$ free electrons per cm^3, Fermi wave number is $k_F=\left(3\pi^2 n_{3D}\right)^{1/3}\simeq 3.1\times10^6\,\mathrm{cm}^{-1}$, and $\lambda_F=2\pi/k_F\simeq 20\,\mathrm{nm}$. So, crudely speaking, an external perturbation in such a medium with a wavelength larger than say 100 nm will not be able to resolve the nonlocality present in the response, hence, such an excitation can enjoy a spatially nondispersive response, $\overline{\overline{\epsilon}}\,(q=0,\omega)$.

2.2. Longitudinal versus Transverse Dielectric Functions

Recall that we choose the excitation to be of a travelling-wave type along the direction $\vec{q}$, so, we split the tensorial DF into longitudinal and transverse parts with respect to the propagation direction of the excitation, $\vec{q}$. Then [12],

$$\overline{\overline{\epsilon}}\,(\vec{q},\omega)=\epsilon_{\parallel}(\vec{q},\omega)\,\frac{\vec{q}\otimes\vec{q}}{q^2}+\epsilon_{\perp}(\vec{q},\omega)\,\left(\overline{\overline{1}}-\frac{\vec{q}\otimes\vec{q}}{q^2}\right). \tag{10}$$

This equation simply means that $\epsilon_{\parallel}(\vec{q},\omega)$ relates the component of the total $\vec{E}$ field along the $\vec{q}$ (i.e., wave propagation) direction to the same component of the displacement field, in other words, a longitudinal relation. Our work concerns only the longitudinal part of the tensorial DF. As a side note, the reason why macroscopic electromagnetic theory is ignorant to the discrimination between the longitudinal and transverse DFs is due to the fact that, in the long wavelength limit these two DFs become equal [12] as:

$$\lim_{\vec{q}\to0}\epsilon_{\perp}(\vec{q},\omega)=\lim_{\vec{q}\to0}\epsilon_{\parallel}(\vec{q},\omega)=\epsilon(\omega). \tag{11}$$

To see the physical significance of the longitudinal DF, we first supplement the Maxwell's equations with the scalar and vector potentials $(V,\vec{A})$ as

$$\vec{B}(\vec{q},\omega)=i\vec{q}\times\vec{A}(\vec{q},\omega), \tag{12}$$

$$\vec{E}(\vec{q},\omega) = \frac{i\omega}{c}\,\vec{A}(\vec{q},\omega) - i\vec{q}\,V(\vec{q},\omega). \tag{13}$$

Of particular importance is the choice of the gauge and in this work we use the Coulomb gauge also known as the transverse or radiation gauges. In the Coulomb gauge we have

$$i\vec{q}\cdot\vec{A}(\vec{q},\omega) = 0. \tag{14}$$

That is, the vector potential is transverse (with respect to wave propagation direction, $\vec{q}$). Then Gauss's law turns into

$$\begin{aligned} 4\pi\rho_{ext}(\vec{q},\omega) &= i\vec{q}\cdot\vec{D}(\vec{q},\omega), \\ &= i\vec{q}\cdot\overline{\overline{\epsilon}}\,(\vec{q},\omega)\,\vec{E}(\vec{q},\omega). \end{aligned} \tag{15}$$

Due to the dot product with $\vec{q}$ only the longitudinal component of $\overline{\overline{\epsilon}}$ is selected, giving

$$4\pi\rho_{ext}(\vec{q},\omega) = i\epsilon_{\parallel}(\vec{q},\omega)\,\vec{q}\cdot\vec{E}(\vec{q},\omega), \tag{16}$$

and using Eq. (13) we obtain for the scalar potential

$$V(\vec{q},\omega) = \frac{4\pi\rho_{ext}(\vec{q},\omega)}{\epsilon_{\parallel}(\vec{q},\omega)\,q^2}. \tag{17}$$

Hence, this equation reminds us that Poisson's equation is also valid for the AC (time-varying) case, provided that we work in the Coulomb gauge. It is important to note that the (screened) scalar potential depends only on the longitudinal DF. Thus the interaction of two electrons via a screened Coulomb potential energy is

$$U_{scr}(\vec{q},\omega) = e^2\frac{4\pi}{\epsilon_{\parallel}(\vec{q},\omega)\,q^2}. \tag{18}$$

In this expression if we identify the electronic charge e as the coupling constant, then the remaining term corresponds to the dressed propagator of a longitudinal photon as

$$D_{\parallel}(\vec{q},\omega) = \frac{4\pi}{\epsilon_{\parallel}(\vec{q},\omega)\,q^2}. \tag{19}$$

For completeness, we also list the dressed transverse photon propagator [12]

$$\overline{\overline{D}}_{\perp}(\vec{q},\omega) = \frac{4\pi c}{\omega^2\,\epsilon_{\perp}(\vec{q},\omega) - q^2\,c^2}\left(\overline{\overline{1}} - \frac{\vec{q}\otimes\vec{q}}{q^2}\right). \tag{20}$$

The poles of the longitudinal and transverse photon propagators determine respectively the longitudinal and transverse eigenmodes of the dielectric medium, which are given by

$$\epsilon_{\parallel}(\vec{q},\omega) = 0, \tag{21}$$

$$\omega^2\,\epsilon_{\perp}(\vec{q},\omega) = q^2\,c^2. \tag{22}$$

These two equations yield the longitudinal and transverse modes that the medium is willing to support, just like an LC resonance circuit that is willing to oscillate at the frequency $\omega_0 = \frac{1}{\sqrt{LC}}$. The main additional requirement of quantum mechanics is that these oscillations should be in discrete packets (quanta) of energy. The quantum of a longitudinal/transverse oscillation of the EL is given the name longitudinal/transverse plasmon. In our work the former plays a decisive role.

3. Auxiliary Functions and Approximation Schemes

Having discussed the basic character of the DF, there remains its computation. This is not an easy task for the EL which is a quantum many-body system; the first successful attempts came not until 1950's, even though the foundations of the solid-state quantum mechanics were laid before 1930's [6].

As in the previous section we consider some arbitrary charge density $\varrho_{ext}(\vec{r},t)$ and the associated current density $\vec{j}_{ext}(\vec{r},t)$. We saw also in the previous section that the longitudinal DF characterizes how charge densities interact, whereas the current density interactions are described by the tensorial transverse DF. As a matter of fact, they are related to density-density and current-current correlation functions, respectively [12]. The EL in response to the external charge density, ϱ_{ext} will screen this perturbation but subject to two important constraints i) Pauli exclusion principle, and ii) Coulomb repulsion among the constituent electrons of the EL. A successful longitudinal DF should take into account these two effects as much as possible. Due to $\varrho_{ext}(\vec{r},t)$, the EL no longer preserves its homogeneity and an induced charge density $\varrho_{ind}(\vec{r},t)$ is produced in response. Hence, the total screened charge density becomes

$$\varrho_{scr}(\vec{r},t) = \varrho_{ext}(\vec{r},t) + \varrho_{ind}(\vec{r},t), \tag{23}$$

which is in reciprocal space

$$\rho_{scr}(\vec{q},\omega) = \rho_{ext}(\vec{q},\omega) + \rho_{ind}(\vec{q},\omega). \tag{24}$$

We denote the corresponding number densities by $n_{scr}(\vec{q},\omega)$, $n_{ext}(\vec{q},\omega)$ and $n_{ind}(\vec{q},\omega)$ with the definition $\rho(\vec{q},\omega) = e\, n(\vec{q},\omega)$ where e denotes the positron charge. These, in turn, generate the potential energies

$$U_{ext}(\vec{q},\omega) = U^0(\vec{q})\, n_{ext}(\vec{q},\omega), \tag{25}$$

$$U_{ind}(\vec{q},\omega) = U^0(\vec{q})\, n_{ind}(\vec{q},\omega), \tag{26}$$

$$\begin{aligned} U_{scr}(\vec{q},\omega) &= U^0(\vec{q})\, n_{scr}(\vec{q},\omega), \\ &= U_{ext}(\vec{q},\omega) + U_{ind}(\vec{q},\omega), \end{aligned} \tag{27}$$

where $U^0(\vec{q})$ denotes the instantaneous bare $1/R$ Coulomb interaction.

3.1. Density Response Function

The following relation is enforced between the external density and the induced den-

sity:

$$n_{ind}(\vec{q},\omega) = \chi(\vec{q},\omega)\, U^0(\vec{q})\, n_{ext}(\vec{q},\omega) = \chi(\vec{q},\omega)\, U_{ext}(\vec{q},\omega), \tag{28}$$

being a linear relation, this restricts our formulation to the linear response framework; that is to say, response to each frequency component of the excitation is assumed to be independent, or in electrical engineering terminology, intermodulation products are ignored under a two-tone excitation. χ here, is referred as the density response function or just as the susceptibility. So, we arrive at the following equation that relates the density response function to the DF

$$\frac{1}{\epsilon(\vec{q},\omega)} = 1 + U^0(\vec{q})\, \chi(\vec{q},\omega). \tag{29}$$

An alternative expression is reached if we introduce the screened density response function by

$$n_{ind}(\vec{q},\omega) = \chi_{scr}(\vec{q},\omega)\, U^0(\vec{q})\, n_{scr}(\vec{q},\omega), \tag{30}$$

as

$$\epsilon(\vec{q},\omega) = 1 - U^0(\vec{q})\, \chi_{scr}(\vec{q},\omega). \tag{31}$$

3.2. Polarization Insertion

Using Feynman's diagrammatic techniques we can reach to direct computation. Accordingly, the screened (dressed) two-body interaction potential $U(\vec{q},\omega)$ using Dyson's equation [13] becomes

$$U_{scr}(\vec{q},\omega) = U^0(\vec{q}) + U^0(\vec{q})\, \pi^*(\vec{q},\omega)\, U_{scr}(\vec{q},\omega). \tag{32}$$

$\pi^*(\vec{q},\omega)$ is the so-called proper polarization insertion. Eq. (32) is represented diagrammatically as in Figure 1.

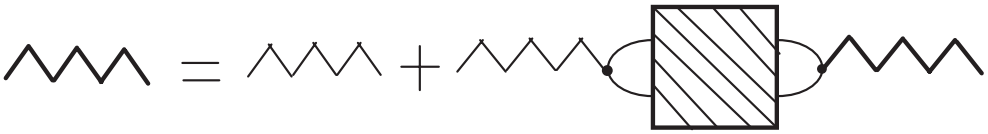

Figure 1. Diagrammatic representation of the Dyson's equation for the dressed insertion, shown by the heavy zig-zag lines and the bare interaction is indicated by the normal zig-zag lines. The sectioned box stands for the proper polarization insertion.

So we get

$$U_{scr}(\vec{q},\omega) = \frac{U^0(\vec{q})}{\epsilon(\vec{q},\omega)} = \frac{U^0(\vec{q})}{1 - U^0(\vec{q})\, \pi^*(\vec{q},\omega)}, \tag{33}$$

which gives

$$\epsilon(\vec{q},\omega) = 1 - U^0(\vec{q})\, \pi^*(\vec{q},\omega). \tag{34}$$

When diagrammatic quantities come into play, a word of caution is generally made regarding causality. The Wick's theorem [13] which underlies Feynman's diagrammatic rules, is applicable to time-ordered operators. However, the real physical quantities (actually the response functions) need to be retarded functions due to the causality principle. For this reason, the diagrammatic quantities, after being computed in time-ordered form should be converted to retarded form using the analytical relation between the two [13].

The equation above reveals that the screened density response function, $\chi_{scr}(\vec{q},\omega)$ corresponds to the proper polarization insertion in the diagrammatic terminology. Similarly, the density response function $\chi(\vec{q},\omega)$ corresponds to the polarization insertion

$$\chi(\vec{q},\omega) = \frac{\chi_{scr}(\vec{q},\omega)}{\epsilon(\vec{q},\omega)} = \pi(\vec{q},\omega). \tag{35}$$

3.3. Random Phase Approximation

Now we are in a position to propose the first approximation for the DF by replacing the $\pi^*(\vec{q},\omega)$ with $\pi^0(\vec{q},\omega)$, where the latter refers to the simple ring diagram without any interaction lines present (see Figure 2), called the noninteracting EL polarization insertion.

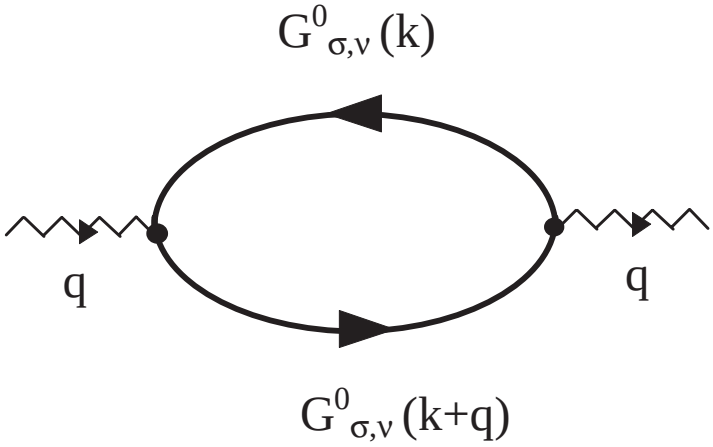

Figure 2. Simple ring diagram, with the spin and valley labels of the electrons indicated.

As π^0 replaces the *proper* polarization insertion, it corresponds to the summation of all ring diagrams for the polarization insertion $\pi(\vec{q},\omega)$. This approximation is the celebrated random phase approximation (RPA) and $\pi^0(\vec{q},\omega)$ is generally called the Lindhard function [14]. Actually "Lindhard" is a generic name but we also use the word "Stern" function for the 2D EL. Equivalently, RPA corresponds to approximating the screened density

response function by the Lindhard function (also to be denoted in this text by $\chi^0(\vec{q},\omega)$). Summarizing the relations for the RPA,

$$\chi^{RPA}_{scr}(\vec{q},\omega) = \chi^0(\vec{q},\omega), \tag{36}$$

$$\epsilon^{RPA}(\vec{q},\omega) = 1 - U^0(\vec{q})\,\chi^0(\vec{q},\omega), \tag{37}$$

$$\chi^{RPA}(\vec{q},\omega) = \frac{\chi^0(\vec{q},\omega)}{1 - U^0(\vec{q})\,\chi^0(\vec{q},\omega)}. \tag{38}$$

The physical outcome of these approximations is that the electrons of the EL are regarded as noninteracting particles but within a field of the external potential as well as the self-consistent average field of the induced charges. So, the many-body effects are to some extend contained in this mean field. However, RPA is well-known to be successful for the long wavelength phenomena. One of the aims of this work is to have a better feeling about the validity range of the widely used RPA.

3.4. Dynamic Local-Field Correction

The RPA density response function (χ^{RPA}) can be corrected by a term called the local-field correction (LFC), denoted by $G(\vec{q},\omega)$, so that, formally the exact density response function (χ) is reached. Stating this in mathematical terms

$$\frac{1}{\chi(\vec{q},\omega)} = \frac{1}{\chi^{RPA}(\vec{q},\omega)} + U^0(\vec{q})\,G(\vec{q},\omega). \tag{39}$$

The mission of $G(\vec{q},\omega)$ is to incorporate the local structure on top of the self-consistent mean-field brought by the RPA. The local structure is due to so-called Pauli and Coulomb holes around each constituent electron of the EL; there exists a neighborhood within which same spin electrons are repelled due to Pauli exclusion principle, furthermore, all electrons are also subject to Coulomb repulsion. Knowing the *exact* LFC is equivalent to knowing the exact density response function. The problem is that, the determination of the LFC is just as difficult.

3.5. Static Local-Field Correction and STLS

As mentioned above the determination of the dynamic LFC is a formidable problem as the exact many-body solution of the EL itself. The common sense, at this point suggests for approximate schemes led by physical guidence. The fundamental and the most crude approximation done is to neglect the frequency dependence of the LFC, i.e., a static LFC, $G(\vec{q})$. As a matter of fact, most of the dielectric formulations of the EL available today are based on a static LFC, and the dynamic case is the challenge for the current front-line researchers [15]. In using a static LFC, basically the inertia of the Pauli-Coulomb hole is neglected. The particular static LFC that we employ in our work has one appealing feature among the other LFC candidates: the static local-field is determined self-consistently. If we include the fact that the mean-field is also self-consistent, this makes a double self-consistency of the effective field.

Without going into its derivation, the static STLS LFC introduced by Singwi, Tosi, Land and Sjölander [16], in D-dimensional space is given by

$$G(\vec{q}) = -\frac{1}{n}\int \frac{d\vec{q}'}{(2\pi)^D}\,\frac{\vec{q}\cdot\vec{q}'}{q^2}\,\frac{U^0(\vec{q}')}{U^0(\vec{q})}\,[S(|\vec{q}-\vec{q}'|)-1]\,, \tag{40}$$

where $S(\cdot)$ is the static form (structure) factor. We refer to Ref. [17] for a detailed derivation of Eq. (40). The static structure factor is related to the DF through

$$S(\vec{q}) = -\frac{\hbar}{n\,\pi\,U^0(\vec{q})}\int_0^\infty d\omega\,\mathrm{Im}\{\frac{1}{\epsilon(\vec{q},\omega)}\}, \tag{41}$$

and the DF depends on the LFC through

$$\epsilon^{LFC}(\vec{q},\omega) = \frac{1-U^0(\vec{q})\,\chi^0(\vec{q},\omega)\,[1-G(\vec{q})]}{1+U^0(\vec{q})\,\chi^0(\vec{q},\omega)\,G(\vec{q})}. \tag{42}$$

So, Eqs. (40)-(42) form a set to be solved self-consistently. As a final remark, Eq.(41) can also be computed by rotating the frequency integration path from real axis to the imaginary axis, resulting in the following alternative expression [18]

$$S(\vec{q}) = \frac{-\hbar}{\pi\,n\,U^0(\vec{q})}\int_0^\infty d\omega\,\left[\frac{1}{\epsilon(\vec{q},i\omega)}-1\right]. \tag{43}$$

4. Expressions for a General $G(q)$

In the following two subsections we provide the governing *explicit* expressions for the EL assuming a general LFC, not necessarily restricted to STLS. However, we also supply the explicit forms for the STLS LFC at the end of each subsection.

4.1. 3D EL Expressions

We first list the expressions relating electron density (n_{3D}), Fermi wave number (k_F), and r_s for an 3D EL with arbitrary spin and valley degeneracy.

$$n_{3D} = \frac{1}{V}\sum_{\vec{k},\sigma,\nu}^{\vec{k}_F,g_s,g_v} n_{\vec{k},\sigma,\nu} = g_s g_v \frac{k_F^3}{6\pi^2}, \tag{44}$$

where V is the volume terminated by periodic boundary conditions and we introduce an overall degeneracy parameter g_d to represent compactly the spin and valley degeneracies, as $g_d = g_s g_v$. Then k_F depends on n_{3D} as

$$k_F = \left(\frac{6\pi^2 n_{3D}}{g_d}\right)^{1/3}. \tag{45}$$

The most important and actually the only parameter in EL theory is r_s defined as the average electron distance in units of the effective Bohr radius, a_B^* of the system

$$n_{3D} = \frac{1}{\frac{4}{3}\pi(r_s a_B^*)^3}, \tag{46}$$

and

$$k_F = \frac{1}{r_s a_B^*}\left(\frac{9\pi}{2g_d}\right)^{1/3}. \tag{47}$$

The effective Bohr radius is given by

$$a_B^* = \frac{\kappa\hbar^2}{m^* e^2}, \tag{48}$$

where κ is the background dielectric constant and m^* is the (isotropic) effective mass of the electrons as introduced in the previous section. a_B^* is an important length-scale and we use it also in 2D EL. The bare $1/R$ Coulomb interaction in reciprocal space is

$$U_{3D}^0(q) = \frac{4\pi e^2}{\kappa q^2}. \tag{49}$$

The dynamo of the DF is still the noninteracting polarization insertion, $\pi^0(q,\omega)$, the Lindhard function. We generalize it for an arbitrary degeneracy factor, g_d. In real space its representation becomes

$$\pi^0(x_1,x_2) = \frac{-i}{\hbar}\sum_{\sigma_1,\sigma_2}\sum_{\nu_1,\nu_2} G^0_{\sigma_1\sigma_2,\nu_1\nu_2}(x_1,x_2)\, G^0_{\sigma_2\sigma_1,\nu_2\nu_1}(x_2,x_1), \tag{50}$$

where G^0 denotes the noninteracting propagator and x_1, x_2 denote both space and time variables. For the homogeneous system at hand working in the reciprocal space is suitable via the Fourier transform which yields

$$\pi^0(\vec{q},\omega_q) = \frac{-ig_d}{\hbar}\int \frac{d^3k\, d\omega_k}{(2\pi)^4} G^0(\vec{k},\omega_k)\, G^0(\vec{q}+\vec{k},\omega_q+\omega_k). \tag{51}$$

We state the result for $U_{3D}^0\,\pi_{3D}^0$ as it always occurs in our expressions in this product form

$$\begin{aligned}\mathrm{Re}\left\{U_{3D}^0(q_n)\,\pi_{3D}^0(q_n,\nu)\right\} = \left(\frac{2g_d^4}{9\pi^4}\right)^{1/3}\frac{r_s}{q_n^2}\Bigg[-1 + \frac{1}{2q_n}(1-\nu_-^2)\ln\left|\frac{1+\nu_-}{1-\nu_-}\right| \\ - \frac{1}{2q_n}(1-\nu_+^2)\ln\left|\frac{1+\nu_+}{1-\nu_+}\right|\Bigg],\end{aligned} \tag{52}$$

$$\mathrm{Im}\left\{U^0_{3D}(q_n)\,\pi^0_{3D}(q_n,\nu)\right\} = -\frac{r_s\pi}{2q_n^3}\left(\frac{2g_d^4}{9\pi^4}\right)^{1/3} \times \begin{cases} (1-\nu_-^2) & \text{for } q_n^2/2+q_n \geq \nu \geq |q_n^2/2-q_n| \\ 2\nu & \text{for } q_n \leq 2 \text{ and } q_n - q_n^2/2 \geq \nu \\ 0 & \text{otherwise} \end{cases} . \quad (53)$$

where we use the reduced units for the wave number and frequency as $q_n = q/k_F$, $\nu = \frac{\hbar\omega}{(2E_F)}$, and

$$\nu_\pm = \frac{\nu}{q_n} \pm \frac{q_n}{2}.$$

We also make use of the Lindhard function with imaginary frequency as mentioned previously; its form in 3D becomes

$$U^0_{3D}(q_n)\,\pi^0_{3D}(q_n,i\nu) = -\frac{r_s}{q_n^2}\left(\frac{2g_d^4}{9\pi^4}\right)^{1/3}\left\{1 - \frac{\nu}{q_n}\tan^{-1}\left[\frac{q_n(2-q_n)}{2\nu}\right] - \frac{\nu}{q_n}\tan^{-1}\left[\frac{q_n(2+q_n)}{2\nu}\right] + \frac{(q_n^2-4)-4(\frac{\nu}{q_n})^2}{8q_n}\ln\left[\frac{(q_n-2)^2+4(\frac{\nu}{q_n})^2}{(q_n+2)^2+4(\frac{\nu}{q_n})^2}\right]\right\}. \quad (54)$$

Using Eqs. (52) and (53) in Eq. (42) the expression for the 3D DF, $\epsilon_{3D}(q_n,\nu)$ is reached; we state the static case that is frequently used

$$\epsilon_{3D}(q_n,0) = \frac{1+\left(\frac{2g_d^4}{9\pi^4}\right)^{1/3}\frac{r_s}{q_n^2}\left(1-\frac{4-q_n^2}{4q_n}\ln|\frac{2-q_n}{2+q_n}|\right)[1-G_{3D}(q_n)]}{1-\left(\frac{2g_d^4}{9\pi^4}\right)^{1/3}\frac{r_s}{q_n^2}\left(1-\frac{4-q_n^2}{4q_n}\ln|\frac{2-q_n}{2+q_n}|\right)G_{3D}(q_n)}. \quad (55)$$

As mentioned in the previous section, there are two possibilities for the computation of the static structure factor, $S(q)$: integration over the real frequency axis (ω) or over the imaginary frequency axis ($i\omega$). The former contains contributions from the electron-hole pair and plasmon excitations as

$$S^{\text{e-h}}_{3D}(q_n) = -\frac{3q_n^2}{2r_s}\left(\frac{9\pi}{2g_d^4}\right)^{1/3}\int_{\nu_{min}(q_n)}^{\nu_{max}(q_n)} d\nu\,\mathrm{Im}\left\{\frac{1}{\epsilon_{3D}(q_n,\nu)}\right\}, \quad (56)$$

where $\nu_{max}(q_n) = q_n^2/2 + q_n$ and $\nu_{min}(q_n) = \max\left\{0\,,\, q_n^2/2 - q_n\right\}$.

$$S^{\text{plas}}_{3D}(q_n) = -\frac{3\pi^2}{2g_d^2}\,q_n^6\frac{1}{r_s^2}\left(\frac{9\pi}{2g_d}\right)^{2/3} \times \frac{\left[1+U^0_{3D}(q_n)\pi^0_{3D}(q_n,\nu)G_{3D}(q_n)\right]^2}{\left[\nu_-\ln\left(\frac{\nu_--1}{\nu_-+1}\right)+\nu_+\ln\left(\frac{\nu_++1}{\nu_+-1}\right)\right]}\,\theta(\nu-\nu_{max}(q_n)), \quad (57)$$

where ν and $\nu_\pm$ in this equation have to be evaluated at the plasmon frequency ν_p, and $\theta(\cdot)$ denotes the unit step function. Finally, the imaginary frequency integration for $S(q)$ simplifies to

$$S_{3D}(q_n) = \frac{3}{2\pi}\int_0^\infty d\nu \frac{\left\{1 - \frac{\nu}{q_n}\tan^{-1}\left[\frac{q_n(2-q_n)}{2\nu}\right] - \frac{\nu}{q_n}\tan^{-1}\left[\frac{q_n(2+q_n)}{2\nu}\right] + \frac{(q_n^2-4)-4(\frac{\nu}{q_n})^2}{8q_n}\ln\left[\frac{(q_n-2)^2+4(\frac{\nu}{q_n})^2}{(q_n+2)^2+4(\frac{\nu}{q_n})^2}\right]\right\}}{1 - U_{3D}^0(q_n)\,\pi_{3D}^0(q_n, i\nu)\,[1 - G_{3D}(q_n)]}. \tag{58}$$

Pair correlation function is the inverse Fourier transform of the static structure factor with the explicit form

$$g_{3D}(r_n) = 1 + \frac{3}{g_d}\int_0^\infty dq_n\,\frac{q_n}{r_n}\sin(q_n r_n)\,[S_{3D}(q_n) - 1]\,, \tag{59}$$

where $r_n = r k_F$. For $r_n = 0$ this expression reduces to

$$g_{3D}(r=0) = 1 + \frac{3}{g_d}\int_0^\infty dq_n\,q_n^2\;[S_{3D}(q_n) - 1]\,. \tag{60}$$

We also state the expression for the statically screened interaction in real space which is the inverse Fourier transform of the corresponding interaction in reciprocal space

$$\overline{U}_{3D,scr}(r_n) = \frac{2}{r_n r_s}\left(\frac{9\pi}{2g_d}\right)^{1/3} + \frac{4}{\pi r_s}\left(\frac{9\pi}{2g_d}\right)^{1/3}\int_0^\infty dq_n \frac{\sin(q_n r_n)}{q_n\, r_n}\left[\frac{1}{\epsilon_{3D}(q_n)} - 1\right], \tag{61}$$

in effective Rydberg units designated by an overbar; we add and subtract unscreened Coulomb potential for computational reasons [19].

Eq. (40) for the STLS LFC can be simplified further in 3D by performing the angular integrations analytically [16], and the final form becomes

$$G_{3D}^{STLS}(q_n) = \frac{3}{2\,g_d}\int_0^\infty dp_n\,p_n^2\;[1 - S(p_n)]\;h_{3D}(a), \tag{62}$$

where $a = p_n/q_n$ and

$$h_{3D}(a) = 1 + \frac{1-a^2}{2a}\ln|\frac{a+1}{a-1}|. \tag{63}$$

We observe that $h_{3D}(a=0) = 2$ and $h_{3D}(a=1) = 1$, so that, it is actually a well-behaved function without singularities. For completeness we would also like to include the expression for the Hubbard LFC for a 3D EL having g_d degeneracy,

$$G_{3D}^{H}(q_n) = \frac{1}{g_d}\,\frac{q_n^2}{1+q_n^2}. \tag{64}$$

The Hubbard LFC [20] approximately accounts for the exchange (Pauli) hole surrounding each electron.

4.2. 2D EL Expressions

We proceed following the same order as in the 3D EL; the expressions relating electron density (n_{2D}), Fermi wave number (k_F), and r_s for an 2D EL with arbitrary spin and valley degeneracy are

$$n_{2D} = \frac{1}{A} \sum_{\vec{k},\sigma,\nu}^{\vec{k}_F,g_s,g_v} n_{\vec{k},\sigma,\nu} = g_d \frac{k_F^2}{4\pi}, \tag{65}$$

where A is the area again terminated by periodic boundary conditions. k_F depends on n_{2D} as

$$k_F = \left(\frac{4\pi n_{2D}}{g_d} \right)^{1/2}. \tag{66}$$

The relation between n_{2D} and r_s is

$$n_{2D} = \frac{1}{\pi (r_s a_B^*)^2}, \tag{67}$$

and

$$k_F = \frac{2}{r_s a_B^*} \frac{1}{\sqrt{g_d}}. \tag{68}$$

In these expressions the effective Bohr radius is the same as the 3D case; that is, the average distance for a $1s$ electron of a 3D hydrogen atom. In the 2D EL the interaction potential in reciprocal space is taken to be

$$U_{2D}^0(q) = \frac{2\pi e^2}{\kappa q}. \tag{69}$$

This potential is obtained by taking the 2D Fourier transform of the 3D Coulomb interaction which is $1/R$, R denoting distance in real space (see for e.g., [21]). In fact a strictly 2D solution of Poisson's equation is proportional to $-\ln(R)$ [22] rather than $1/R$ and its 2D Fourier transform is proportional to $1/q^2$ as in 3D EL. However, the $-\ln(R)$ interaction is seldom used [23] due to indication by real physical 2D systems that $1/R$ type of interaction is relevant [24, 2].

Remembering that the 3D polarization insertion is named after Lindhard, it is appropriate to name the 2D zeroth-order polarization insertion as the Stern function in honor of Frank Stern who first worked out its explicit form [25, 26]. Again we state the $U_{2D}^0 \pi_{2D}^0$ as it always occurs in our expressions in this product form

$$\begin{aligned} \mathrm{Re}\left\{ U_{2D}^0(q_n)\, \pi_{2D}^0(q_n,\nu) \right\} = \frac{r_s g_d^{3/2}}{2} \frac{1}{q_n} \Bigg[-1 - \frac{\mathrm{sgn}(\nu_-)}{q_n}\, \Theta(|\nu_-|-1) \sqrt{\nu_-^2 - 1} \\ + \frac{\mathrm{sgn}(\nu_+)}{q_n}\, \Theta(|\nu_+|-1) \sqrt{\nu_+^2 - 1} \Bigg], \end{aligned} \tag{70}$$

$$\mathrm{Im}\left\{U_{2D}^{0}(q_n)\,\pi_{2D}^{0}(q_n,\nu)\right\}=\frac{r_s g_d^{3/2}}{2}\frac{1}{q_n^2}\left[\Theta(1-|\nu_+|)\sqrt{1-\nu_+^2}-\Theta(1-|\nu_-|)\sqrt{1-\nu_-^2}\right], \tag{71}$$

where we use the same definitions for the reduced variables q_n and $\nu_\pm$ as in the previous section, and sgn$(\cdot)$ denotes the signum (sign) function. The 2D static DF with a general LFC becomes

$$\epsilon_{2D}(q_n,0)=\begin{cases}\dfrac{1+\dfrac{g_d^{3/2}r_s}{2q_n}\left[1-G_{2D}(q_n)\right]}{1-\dfrac{g_d^{3/2}r_s}{2q_n}G_{2D}(q_n)} & \text{for } q_n\le 2\\[2ex] \dfrac{1+\dfrac{g_d^{3/2}r_s}{2q_n}\left[1-\sqrt{1-(\dfrac{2}{q_n})^2}\right]\left[1-G_{2D}(q_n)\right]}{1-\dfrac{g_d^{3/2}r_s}{2q_n}\left[1-\sqrt{1-(\dfrac{2}{q_n})^2}\right]G_{2D}(q_n)} & \text{for } q_n>2\end{cases}. \tag{72}$$

In calculating the static structure factor, $S(q)$ we have two choices, the conventional approach is to separately account for the electron-hole pair and plasmon contributions as

$$S_{2D}^{\text{e-h}}(q_n)=-\frac{4q_n}{\pi r_s g_d^{3/2}}\int_{\nu_{min}(q_n)}^{\nu_{max}(q_n)}d\nu\;\mathrm{Im}\left\{\frac{1}{\epsilon_{2D}(q_n,\nu)}\right\}, \tag{73}$$

where again $\nu_{max}(q_n)=q_n^2/2+q_n$ and $\nu_{min}(q_n)=\max\left\{0\,,\;q_n^2/2-q_n\right\}$;

$$S_{2D}^{\text{plas}}(q_n)=-\frac{8q_n^4}{r_s^2 g_d^3}\frac{\left[1+U_{2D}^{0}(q_n)\,\pi_{2D}^{0}(q_n,\nu)\,G_{2D}(q_n)\right]^2}{\left[\frac{\nu_+}{\sqrt{\nu_+^2-1}}-\frac{\nu_-}{\sqrt{\nu_-^2-1}}\right]}\,\theta(\nu-\nu_{max}(q_n)), \tag{74}$$

where ν and $\nu_\pm$ in this equation have to be evaluated at the plasmon frequency ν_p; in contrast to 3D case the plasmon dispersion can be obtained in closed form as [27]

$$\nu_p(q_n)=\frac{q_n(z+1)}{2}\left[q_n^2+\frac{4}{z^2+2z}\right]^{1/2}, \tag{75}$$

with z defined as

$$z=\frac{2q_n}{r_s g_d^{3/2}\,\left[1-G_{2D}(q_n)\right]}. \tag{76}$$

Eq. (75) is valid in the range $[0,q_{n,max}]$ where $q_{n,max}$ satisfies $\nu_p(q_{n,max})=q_{n,max}+q_{n,max}^2/2$ and outside this region plasmons dissociate to electron-hole pairs so that collective excitations are no longer long-lived. The other alternative for computing $S_{2D}(q_n)$ makes use of the Stern function with imaginary frequency, however, we further apply the

so-called Ioriatti-Isihara transformations [28, 29, 2] which greatly simplifies calculation to the form

$$S_{2D}(q_n) = \frac{q_n^2}{\pi} \int_0^{\alpha(q_n)} d\theta \frac{\left[\frac{4}{q_n^2} - \sin^2\theta + \frac{4\cot^2\theta}{q_n^2}\right] (1-\cos\theta)}{\left(\frac{4}{q_n^2} - \sin^2\theta\right)^{1/2} \left[1 + \frac{g_d^{3/2} r_s}{2q_n}(1-\cos\theta)\,(1 - G_{2D}(q_n))\right]}, \quad (77)$$

where

$$\alpha(q_n) = \begin{cases} \pi/2 & \text{for } q_n \le 2 \\ \sin^{-1}\left(\frac{2}{q_n}\right) & \text{for } q_n > 2 \end{cases}. \quad (78)$$

In the numerical computation one should use

$$\cot^2\theta\,(1-\cos\theta) \simeq \frac{1}{2}\left(1 - \frac{9}{12}\theta^2\right) \text{ for } 0 \le \theta \le 0.1,$$

where θ is in radians; otherwise the term $\cot^2\theta$ alone will cause a problem for $\theta \to 0$. However, the second approach based on Eq. (77) becomes numerically very sensitive and costly for $q_n > 2$, for this reason we switch to ordinary approach (Eq. (73)) after the plasmon excitations become Landau-damped.

The 2D pair correlation function and statically screened interaction in real space are obtained as

$$g_{2D}(r_n) = 1 + \frac{2}{g_d} \int_0^\infty dq_n\, q_n\, \mathrm{J}_0(q_n r_n)\,[S_{2D}(q_n) - 1], \quad (79)$$

$$\overline{U}_{2D,scr}(r_n) = \frac{4}{r_s\sqrt{g_d}\, r_n} + \frac{4}{r_s\sqrt{g_d}} \int_0^\infty dq_n\, \mathrm{J}_0(q_n r_n) \left[\frac{1}{\epsilon_{2D}(q_n)} - 1\right], \quad (80)$$

where J_0 is the zeroth-order cylindrical Bessel function of the first kind.

Finally, for the STLS LFC in the 2D case, the polar integral of Eq. (40) cannot be expressed in terms of elementary functions, so the computation becomes slightly more involved. The explicit form is

$$G_{2D}^{STLS}(q_n) = \frac{2}{g_d} \int_0^\infty dp_n\, p_n\, [1 - S(p_n)]\; h_{2D}(a), \quad (81)$$

where $a = p_n/q_n$ and

$$h_{2D}(a) = \frac{1}{\pi} \int_0^\pi d\phi\, \frac{a\cos\phi + 1}{\sqrt{1 + a^2 + 2a\cos\phi}}. \quad (82)$$

The asymptotical form of $h_{2D}(a)$ is $\frac{1}{2a}$, which can safely be used for $a \ge 10$. To reduce the computational labour, we tabulate the function $h_{2D}(a)$ in the interval $[0, 10]$ using 1000 data points, thereby, the burden of the double integration is circumvented.

Finally, the expression for the Hubbard LFC in 2D case is

$$G^H_{2D}(q_n) = \frac{1}{g_d} \frac{q_n}{\sqrt{1+q_n^2}}. \tag{83}$$

5. Results for Structure-Related Quantities

In this section we gather the results pertaining the formulation given in the previous sections. For 3D EL, we compare the STLS results with the recent quantum Monte Carlo (QMC) data released by two groups working in this field [9, 30]. Currently, QMC is believed to yield the most accurate data, however, the agreement between the QMC results produced by independent groups is not satisfactory, and moreover, the computational cost severely restricts the output to a very coarse data grid. Among the exhaustive list of available LFCs [15], the approach due to David Pines, who contributed heavily to this field, and his co-workers [31] deserves special respect and we include in our comparison their pseudopotential formulation [32, 33], which renders our treatment more interesting and complete. Our results indicate that STLS, with its comparatively low computational cost and apart from some drawbacks to be mentioned, offers to be a good alternative.

The 2D EL is given a special emphasis in this work due to its technological importance. Again we compare the 2D STLS results with the QMC data produced by two independent groups [34, 35]. This time we also have the opportunity to test the spin-polarized STLS results with the QMC data of Tanatar and Ceperley [34]. Again our comparison is supplemented by the pseudopotential approach which was pursued for 2D EL by Iwamoto [21].

5.1. 3D EL Results

Our reference in comparing the STLS DF is the QMC data recently produced by two independent groups [9, 30]. This choice is due to the currently existent confidence on the QMC data. As a matter of fact, our investigation does not only question STLS but the QMC results as well, by comparing the agreement of the data produced by these two independent groups. We do not make use of the full strength of the formulation developed in the previous sections; the comparison will involve only the normal-state of the single-valley EL ($g_d = 2$), due to lack of QMC data for other degeneracy factors.

The longitudinal plasmon dispersion extracted from the zeros of the STLS DF is shown in Figure 3 for several r_s values. In this figure, the plasmon energy is normalized to Fermi energy and the wave number is normalized to Fermi wave number. The plasmon dispersion curves are mainly included to assist future researchers for comparing their own data. The plasmon curves are shown till the dotted line which marks the onset of the single electron-hole pair production. Within this region, the imaginary part of the DF is not zero, however, the zeros of the real part of the DF can still be traced, even though, the plasmon will not be a long-lived elementary excitation due to Landau-damping. It needs to be mentioned that most of the techniques including STLS, out of the single- pair

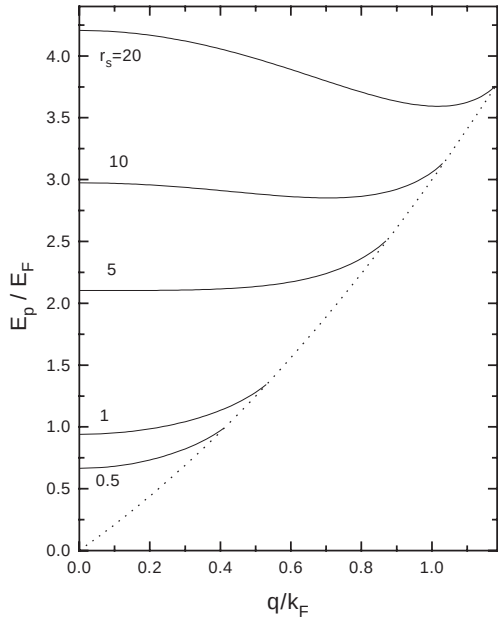

Figure 3. Plasmon energy (E_p) normalized to Fermi energy (E_F) versus q/k_F, of the 3D EL based on STLS. The dotted line marks the onset of particle-hole continuum.

continuum, predict undamped plasmons. However, experiments indicate a finite lifetime possibly due to two effects that are usually omitted: multipair excitations which are not restricted to the single-pair continuum zone, and the interaction of the electrons with the periodic lattice potential [36].

Bowen *et al.* [9] reported their QMC data on the static DF for the 3D EL at the densities $r_s = 1$, 4, 6 and 10. Soon afterwards, Moroni *et al.* [30] announced their QMC results on the static LFC of the 3D EL, computed at the r_s values 2, 5 and 10. First, we extract $G(q)$ (actually $G(q,0)$) data from the tabulated $\epsilon^{-1}(q,0)$ data of Bowen *et al.* by means of the equation

$$G(\vec{q},\omega) = \frac{1}{1-\epsilon(\vec{q},\omega)} - \frac{1}{U^0(\vec{q})\,\chi^0(\vec{q},\omega)}. \tag{84}$$

We should note that this equation is exact. Thereby, we can compare $G(q)$ of STLS with the two QMC data, as shown in Figure 4. In these Figures we also include the LFC based on Pines and Iwamoto's pseudopotential theory [32]. In adapting the liquid Helium formulation to EL problem, Iwamoto and Pines (IP) essentially constrained the static LFC, so that certain static response functions of the EL coincide with the "accurate" QMC data. In particular, they fitted their static LFC to the long-wavelength limit

($q \to 0$) of the compressibility and spin susceptibility QMC data of Ceperley and Alder [37]. The resultant form of the LFC can be named as a generalized Hubbard LFC, as it also incorporates the correlation among spin antiparallel($\uparrow\downarrow$) electrons as well as the parallel spin ($\uparrow\uparrow$) ones,

$$G_{3D}^{IP}(q_n) = \underbrace{\frac{q_n^2}{2\left(q_n^2 + q_{\uparrow\uparrow}^2\right)}}_{\text{Exchange}} + \underbrace{\frac{q_n^2}{2\left(q_n^2 + q_{\uparrow\downarrow}^2\right)}}_{\text{Ex.-Corr.}}. \tag{85}$$

We should mention that the ordinary Hubbard LFC is obtained from this form by setting $q_{\uparrow\uparrow} \to \infty$ (i.e., no correlation) and $q_{\uparrow\downarrow} \to 1$ (exchange part). However, IP's LFC reduces for $r_s \to 0$ (exchange dominant regime) to the form [32]

$$G_{3D}^{IP\to H}(q_n) = \frac{1}{2}\frac{q_n^2}{q_n^2 + 2}; \tag{86}$$

This is nothing but the form suggested by Geldart and Vosko [38] by correcting Hubbard's original LFC. The values for $q_{\uparrow\uparrow}$ and $q_{\uparrow\downarrow}$ are tabulated by IP in the density range r_s =1-20.

Having made this introduction for the pseudopotential theory of IP we can make the following observations about the Figure 4: i) STLS and the QMC data due to Bowen *et al.* denoted by *QMC (1)* have a reasonable agreement for all r_s values given. $G(q)$ due to *QMC (1)* is observed to be consistently lower than that of the STLS values. ii) The QMC data of Moroni *et al.* which will be represented by *QMC (2)* is reported for $q_n = q/k_F$ values larger than 1. The agreement of $G(q)$ with STLS is especially poor for $q_n > 2$ for all r_s values. We believe this to be an artifact of STLS in accounting for the short-range correlations. However, we would like to draw attention to the case $r_s = 10$, where a direct comparison of the two QMC data is possible. There, we observe that *QMC (2)* increasingly disagrees with *QMC (1)* for large q_n values. The IP LFC fitted to QMC data in the long-wavelength, as expected agrees with QMC in the $q_n \to 0$ region much better than STLS. However, this picture quickly changes; for the intermediate q_n values STLS is superior to IP.

Figure 5 illustrates the inverse static DFs of the STLS and the QMC. The agreement of STLS with *QMC (1)* is good for $r_s = 1$ and 4 values, but for the case of $r_s = 6$ and especially for $r_s = 10$, there is a disagreement for the long wavelengths $q_n \leq 1.5$. In this region STLS shows an exaggerated *overscreening* (i.e., $\epsilon < 0$) as compared to QMC. Even though, formally both of the techniques are to be questioned, we again blame STLS due to its violation of the compressibility sum rule [16, 5], which is manifested in the long wavelength behavior of the static DF. We elaborate more on this subject while analyzing the 2D EL. Another interesting point is that the sizeable disagreement of STLS and QMC in the $G(q)$ data for $r_s = 10$ and $q_n > 2$ values is not reflected on $\epsilon^{-1}(q)$ results, where this time an excellent agreement is recorded for $q_n \geq 1.5$ between the two. In Figure 5 (b) the RPA result is also included to show its failure for all practical wave numbers. IP again shows a good agreement with the QMC data only in the extreme long-wavelength

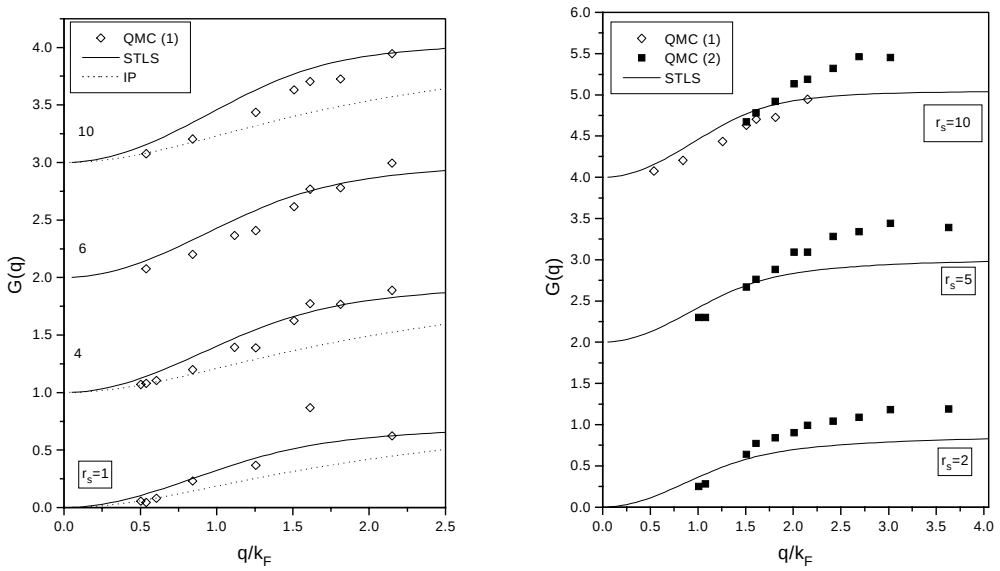

Figure 4. $G(q)$ versus q/k_F. (a) Diamonds show QMC data extracted from the work of Bowen and co-workers, dotted lines refer to Iwamoto and Pines' (IP) LFC, (b) solid squares show the QMC data of Moroni and co-workers. The upper curve also compares the two independent QMC results and STLS, where solid lines indicate STLS results. The curves in (a) and (b) are vertically offset by 1 and 2 units respectively for clarity.

limit; for $r_s = 6$, IP results are not included in the comparison as $q_{\uparrow\uparrow}$ and $q_{\uparrow\downarrow}$ values are not supplied by IP at this r_s value. Finally, the disagreement of the two independent QMC data and the few number of data points available due to computational cost of the simulation, lead us to conclude that QMC is still premature, and in 3D, STLS seems to be a better alternative for practical screening applications together with its limitations. The IP pseudopotential approach shows a complementary performance to that of STLS, where only in the long-wavelength limit a good agreement with QMC is registered.

5.2. 2D EL Results

Our assessment of the DFs for the 2D EL is more comprehensive than the 3D case. Our comparison again includes the STLS, QMC and the pseudopotential theory which was undertaken by Iwamoto for the 2D EL. For the QMC data we have two independent simulations due to Tanatar and Ceperley (TC) [34] (to be abbreviated by QMC-TC) and very recently by Senatore [39, 35] (QMC-S). The former is among the most cited works in EL theory due to the exhaustive and accurate treatment, moreover, we have the

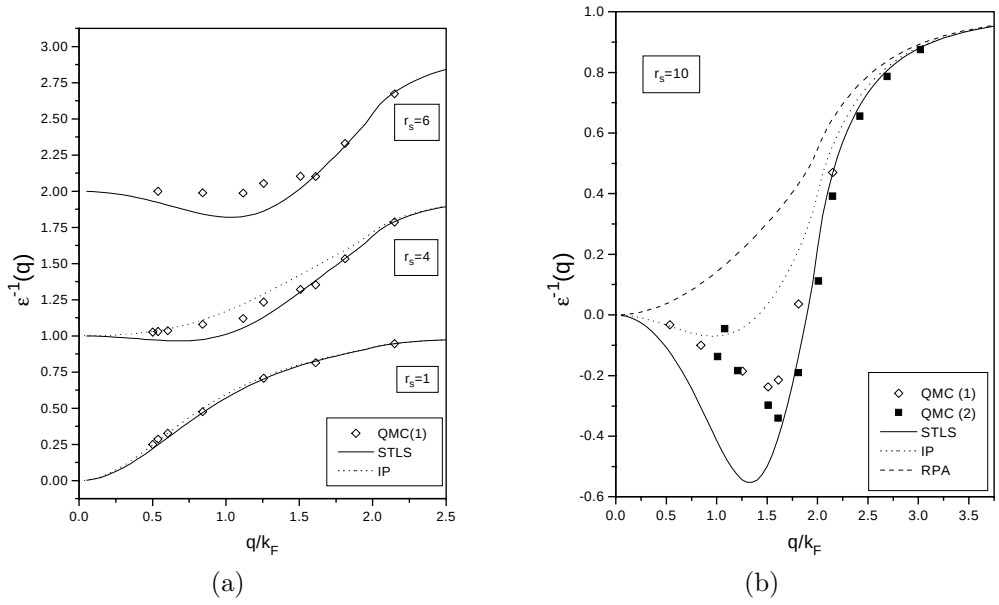

Figure 5. Inverse static DF versus q/k_F. (a) Diamonds show QMC data of Bowen and co-workers and solid lines indicate STLS results for r_s=1, 4, 6. (b) Comparison of the static DF for $r_s = 10$. Additionally, solid squares show the results extracted from the QMC data of Moroni and co-workers and dashed line indicates the RPA result. The dotted lines refer to Iwamoto and Pines' (IP) LFC. The upper curves in (a) are vertically offset by 1 unit for clarity.

opportunity to make use of our general formulation by comparing the spin-polarized EL as well.

In Figures 6 and 7 we first compare the STLS $g(r)$ and $S(q)$ data with QMC-TC in the density range $r_s = 1 - 20$ for both the normal ($g_d = 2$) and spin-polarized ($g_d = 1$) states of the EL. If we first concentrate on the QMC data, and compare the effect of the degeneracy factor g_d on $g(r)$ and $S(q)$, we observe that for r_s =1 and 5 the differences are marginal, apart from $g(0)$ values, where the spin-polarized state goes to zero even for $r_s = 1$ case as expected. Another observation is that the spin-polarized state has a more pronounced structure for $r_s = 10$ and 20 values. For both states STLS results are in excellent agreement with the QMC-TC for r_s =1 and 5. However, especially for r_s =20 the peaks signifying an approach towards crystallization are very much underestimated by the STLS. So, in the search for the Wigner solid, which is predicted to be around $r_s \simeq 37$ [34], STLS falls far short; see also our work for further supports [26]. However, such r_s values are well beyond the practical region utilized by electronic devices and materials. We also indicate in $S(q)$ curves for g_d =2, the plasmon contribution for r_s=1; observe that in the long-wavelength limit $S(q)$ is dominated by the plasmon contribution

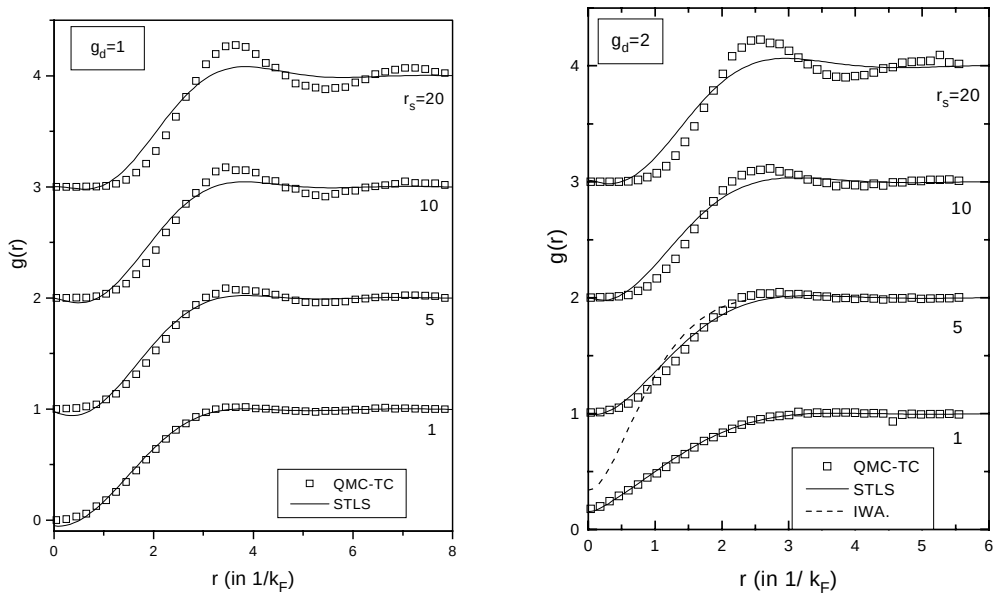

(a) (b)

Figure 6. Pair-correlation function versus distance for $r_s = 1 - 20$. Hollow squares indicate the QMC data of TC, solid curves are STLS results for a) spin-polarized EL ($g_d = 1$). Upper curves are successively shifted vertically by one unit for clarity. Dotted curve on the right shows Iwamoto's result for $r_s = 5$.

as compared to single-pair and multi-pair contributions.

Figures 8 to 10 compare LFC and static DF for STLS, QMC-S (Senatore) and pseudopotential approaches. Iwamoto fitted the 2D LFC to the long-wavelength behavior of the compressibility and spin susceptibility data of QMC-TC. The resultant form of the Iwamoto's LFC is again a generalization of the Hubbard LFC in 2D as,

$$G^I_{2D}(q_n) = \underbrace{\frac{q_n}{2\sqrt{q_n^2 + q_{\uparrow\uparrow}^2}}}_{\text{Exchange}} + \underbrace{\frac{q_n}{2\sqrt{q_n^2 + q_{\uparrow\downarrow}^2}}}_{\text{Ex.-Corr.}} . \tag{87}$$

The values for $q_{\uparrow\uparrow}$ and $q_{\uparrow\downarrow}$ are tabulated by Iwamoto in the density range r_s=1-40.

The bottleneck about the *static* LFCs has been emphasized in another work of Iwamoto [40]; namely the compressibility sum-rule and the third-frequency moment sum rule [15] cannot be satisfied simultaneously by *static* LFCs. So, depending on the particular application at hand, one should choose a suitable static LFC which performs well for that specific physical quantity of interest. Iwamoto's LFC is appealing for our considerations

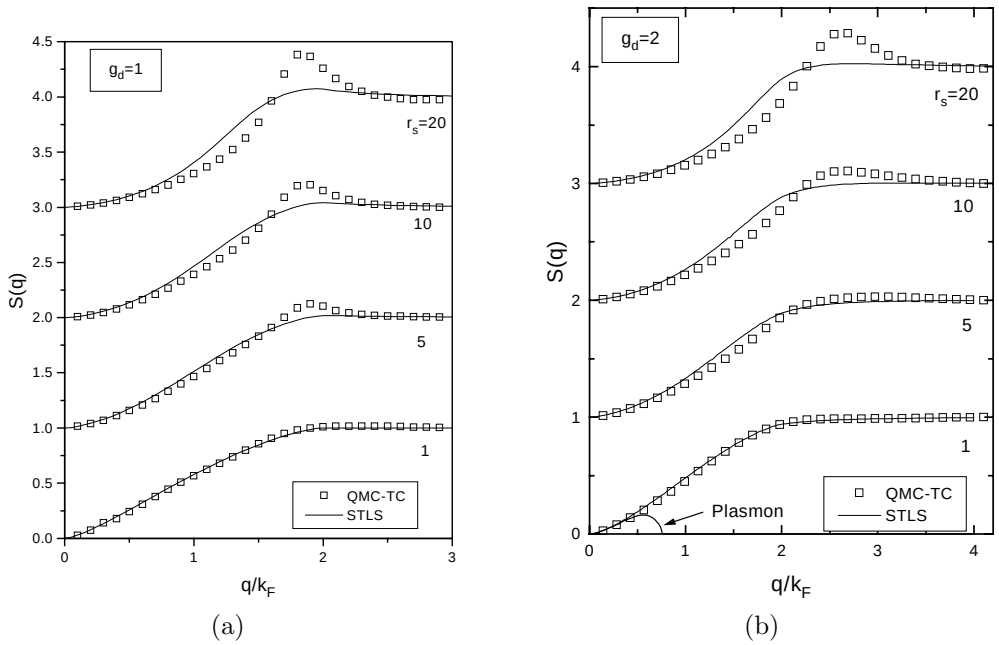

Figure 7. Static form factor versus normalized wave number for $r_s = 1 - 20$. Hollow squares indicate the QMC data of TC, solid curves are STLS results for a) spin-polarized EL ($g_d = 1$). Upper curves are successively shifted vertically by one unit for clarity. The STLS plasmon contribution to the overall form factor is indicated on the right for the $r_s = 1$ case.

as it is fitted to the long-wavelength compressiblity of the QMC data where STLS is known to be very weak. Our following investigation illuminates this dark spot by comparing the two extreme static LFCs by the QMC data. On one side we have STLS that violates the compressibility sum rule but has an impressive pair correlation function due to the built-in self-consistency and on the other hand the pseudopotential approach that presumably behaves just the opposite way.

Our observations about Figures 8 to 10 can be listed as follows: i) Iwamoto's pseudopotential approach only agrees with the QMC-S in the long-wavelengths, where STLS is observed to be in disagreement, ii) for intermediate wave numbers STLS and QMC-S agree very well apart from the fluctuations of the latter, ii) for large wave numbers QMC-S and STLS disagree for $G(q)$ data, where STLS saturates but QMC continues to grow. However, this disagreement is not reflected to the static DF data which shows a good agreement of the two. As a matter of fact, we had similar observations about the static performances of these three aprroaches in 3D case.

Both Iwamoto-Pines [32] and Iwamoto papers do not present any quantitative assessment of their pair-correlation function. We explore this for the 2D case in Figure 11 by

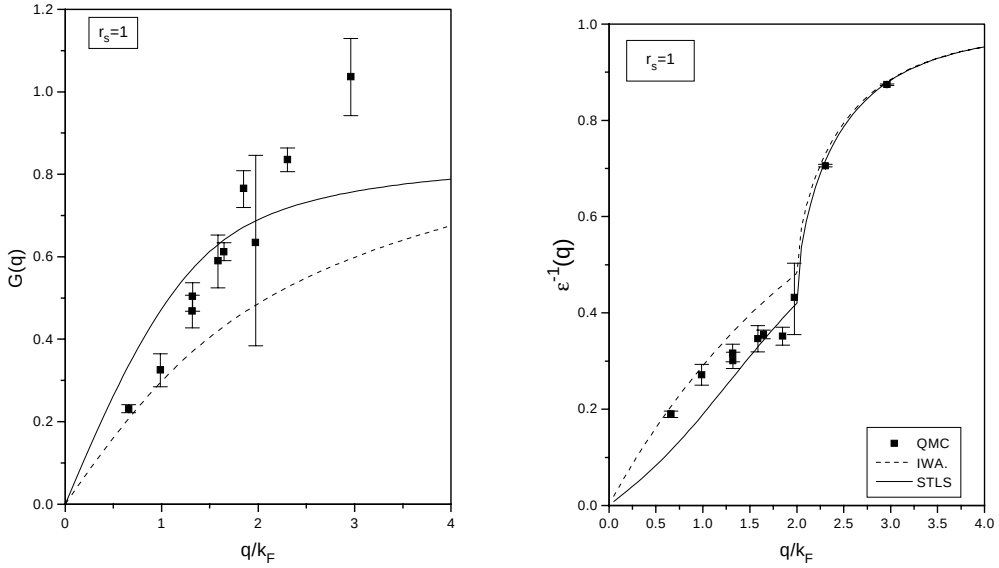

Figure 8. Comparison of STLS (solid lines), QMC-S (squares) and pseudopotential approach of Iwamoto (dashed lines) for the a) LFC and b) inverse static DF of a 2D EL with $g_d = 2$ at $r_s = 1$.

comparing $g(r)$ of STLS and Iwamoto; also see $r_s = 1$ curve in Figure 6 (b). $g(r)$ for small r values as calculated from Iwamoto's LFC is seen to be increasingly negative for increasing r_s values; STLS practically preserves its nonnegative property for all r_s values. In summary, STLS, apart from its deteriorated long-wavelength behavior has several appealing features: i) good agreement with QMC for intermediate and large q values for the static DF over all realistic r_s values, ii) almost nonnegative pair-correlation function, and the most important of all, iii) self- consistent scheme which does not require any fitting to experimental or simulation data (in contrast to pseudopotential approach). This last property makes STLS a highly preferred technique for characterizing quantum liquids with arbitrary geometrical constraints such as heterojunctions, quantum wells, quantum wires and etc., where QMC data is not available.

6. Correlation Energy of the 2D Electron Liquid

Wigner defined the correlation energy *per electron* of the EL as

$$E_{corr} = E_g - E_g^{HF}, \tag{88}$$

where E_g is the ground-state energy (per electron) of the EL and E_g^{HF} is the ground-state

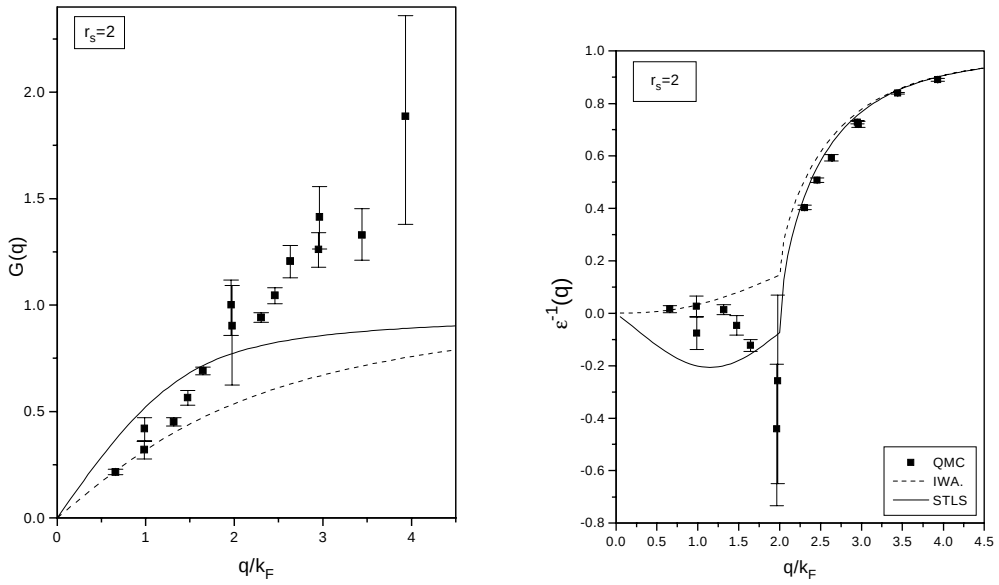

Figure 9. Same as the previous figure but at $r_s = 2$.

energy (per electron) in Hartree-Fock (HF) approximation. The difference between the two lies in the many-body wave functions that characterize the ground-state of the EL: the former considers the *exact* ground-state, $|\Psi_g\rangle$, i.e., $E_g = \langle\Psi_g|H = \hat{T} + \hat{U}|\Psi_g\rangle$ and the latter assumes the ground-state of the EL to be that of the *noninteracting* EL, which is the filled Fermi sea, $|\mathrm{F}\rangle$, i.e., $E_g^{HF} = \langle\mathrm{F}|H|\mathrm{F}\rangle$. E_g^{HF} can be splitted into the kinetic and potential energy terms as

$$E_g^{HF} = \langle\mathrm{F}|\hat{T}|\mathrm{F}\rangle + \langle\mathrm{F}|\hat{U}|\mathrm{F}\rangle = E_{kin}^{HF} + E_{ex}^{HF}. \tag{89}$$

The potential energy for the filled Fermi sea is the Coulomb interaction between equal spin electrons and for this reason it is abbreviated as *ex* standing for exchange.

The correlation energy is calculated by treating the Hamiltonian artificially as $\hat{H}(\lambda) = \hat{T} + \lambda\hat{U}$ and performing an integration over the coupling constant λ and subtracting the HF exchange energy. That is,

$$E_{corr} = \int_0^1 \frac{d\lambda}{\lambda} E_{int}(\lambda) - E_{ex}^{HF}, \tag{90}$$

where

$$E_{int}(\lambda) = \langle\Psi_g(\lambda)|\lambda\hat{U}|\Psi_g(\lambda)\rangle. \tag{91}$$

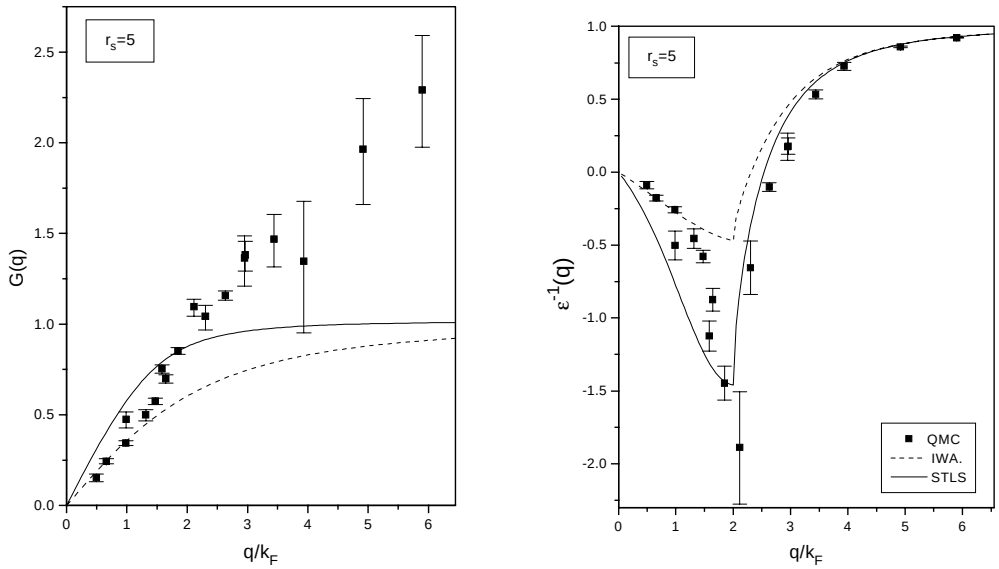

Figure 10. Same as the previous two figures but at $r_s = 5$.

We do not include the details of the calculation; for the details Mahan's book can be referred for the 3D El [5] and Iwamoto's paper includes both 3D and 2D ELs [40]. The final form for the correlation energy of the 2D EL having $g_d = 2$ is

$$E_{corr,2D} = \underbrace{-\frac{2\sqrt{2}}{r_s^2}\int_0^{r_s} dr'_s\,\gamma(r'_s)}_{\text{Exchange-correlation En.}} + \underbrace{\frac{8\sqrt{2}}{3\,\pi\,r_s}}_{-E^{HF}_{ex,2D}}, \tag{92}$$

where

$$\gamma(r'_s) = \frac{1}{2}\int_0^{\infty} dq_n\ \left[1 - S_{r'_s}(q_n)\right]. \tag{93}$$

Note that to determine the correlation energy at a density r_s, we need to know the static form factor at all intermediate r'_s values between 0 to r_s. For this reason the computation of the correlation energy and therefore the compressibility (see the next section) of the EL becomes a costly task. Figure 12 (a) and (b) illustrate the ground-state energy and the correlation energy of the 2D EL again under several approaches. Notably, we indicate in Figure 12 (a) the gas-liquid transition density as the point where the ground-state energy becomes negative. Having made this choice which is somewhat arbitrary (see Isihara [2]), all approaches (including the Hartree-Fock) yield a value about $r_s = 0.7$ for this

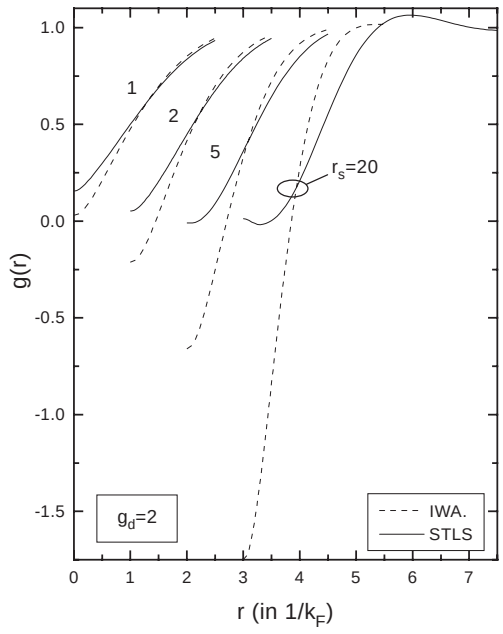

Figure 11. Comparison of the pair-correlation functions of the STLS (solid lines) and the pseudopotential appproach of Iwamoto (dashed lines) for several densities of the 2D EL with $g_d = 2$. Curves are successively shifted horizontally by one unit to the right for clarity.

transition density, however, in this work we use the word *liquid* for all densities without discrimination.

7. Isothermal Compressibility of the 2D Electron Liquid

Isothermal compressibility is a thermodynamic quantity; it describes an important macroscopic property of the system. Our system is the EL; imagine now that we want to compress this system, keeping the temperature (i.e., isothermal) and particle number inside constant. We must overcome basically two kinds of forces: one is the pressure exerted on the bounding walls of the system due to the kinetic energy of the electrons, the other is the interparticle Coulomb and exchange forces that resist to compression. To explain the latter just recall that equal-spin particles do not like to get closer in space, which the compression wants to achieve.

Again we do not include the intermediate steps (see [5, 40]) but present only the final expression for the compressiblity of the 2D EL.

$$\frac{K_{2D}^0}{K_{2D}} = 1 - \frac{\sqrt{2}r_s}{\pi} + \frac{1}{8}\left[-r_s^3\,\frac{\partial E_{corr,2D}}{\partial r_s} + r_s^4\,\frac{\partial^2 E_{corr,2D}}{\partial r_s^2}\right], \tag{94}$$

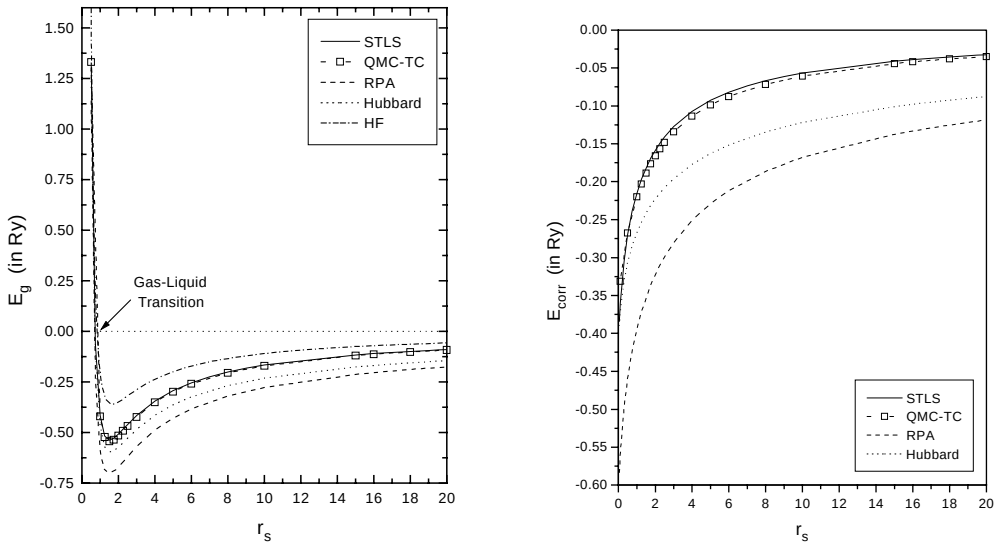

Figure 12. a) the ground-state energy and b) the correlation energy (both in Rydbergs) of the 2D EL with $g_d = 2$ versus r_s using several techniques as indicated (HF stands for Hartree-Fock).

where $E_{corr,2D}$ in this expression should be in Rydberg units, and K_{2D}^0 is the isothermal compressibility of the 2D free Fermi gas, which is used for normalization purposes. We consider the *inverse* compressiblity (just as in the inverse static DF case) due to the ease in plotting this quantity rather than the reciprocal. Observe that, having determined the correlation energy, we additionally require a double differentiation with respect to r_s to get the compressibility expression.

There is an alternative method of determining the isothermal compressibility which is much easier to compute once the static DF is known. This is an *exact* relation between the compressiblity and the long-wavelength limit of the static DF given as [5]

$$\lim_{q\to 0} \epsilon(q,0) = 1 + U^0(q)\, n^2\, K, \tag{95}$$

where n is the particle density, and this relation is valid for any dimensions. The normalized compressibility in terms of the static DF for 2D EL becomes

$$\frac{K_{2D}}{K_{2D}^0} = \lim_{q\to 0} \left\{ \frac{q}{q_{TF}} \left[\epsilon(q,0) - 1\right] \right\}, \tag{96}$$

where $q_{TF} = 2/a_B^*$ is the Thomas-Fermi wave number for 2D EL (with $g_d = 2$). We now list the specific forms of the normalized inverse compressibility for the choices of RPA,

Hubbard and STLS:

$$\left(\frac{K_{2D}^0}{K_{2D}}\right)_{RPA} = 1, \tag{97}$$

$$\left(\frac{K_{2D}^0}{K_{2D}}\right)_{Hub.} = 1 - \frac{r_s}{\sqrt{2}}, \tag{98}$$

$$\left(\frac{K_{2D}^0}{K_{2D}}\right)_{STLS} = 1 - \sqrt{2}\, r_s\, \gamma(r_s), \tag{99}$$

where $\gamma(r_s) = \frac{1}{2}\int_0^\infty dq_n\, [1 - S(q_n)]$. Also note that the RPA static DF in the long-wavelength limit behaves just like the noninteracting Fermi gas so that the ratio comes out as unity.

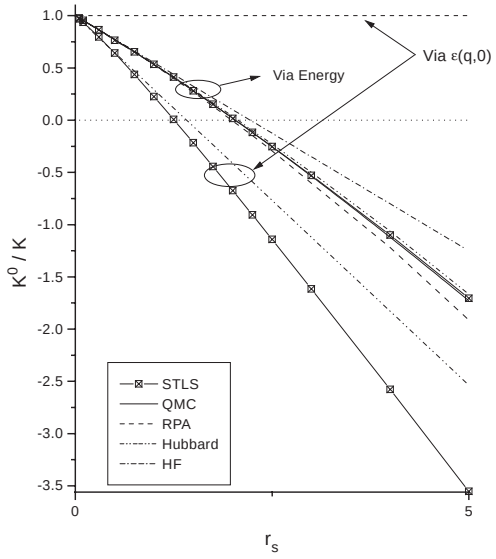

Figure 13. The isothermal compressibility of the 2D EL with $g_d = 2$ versus r_s using several techniques (HF stands for Hartree-Fock). Two alternative approaches, the energy differentiation and long-wavelength static DF are used as indicated.

In summary, we have two choices for computing the compressibility of the EL and they should yield the same result; this requirement is called the *compressibility sum-rule*. The inevitably approximate nature of the DFs cause the violation of this rule by most of them. We illustrate this point in Figure 13 by calculating the normalized inverse compressiblity using the energy and the long-wavelength static DF approaches. As in the 3D EL case [5] STLS violates the compressibility sum-rule which was in fact, reflected in the poor agreement with the QMC data in the long- wavelengths.

8. Overscreening

Figure 13 illustrates that all of the techniques (other than RPA via static DF) agree upon the fact that eventually the compressibility of the 2D EL becomes *negative*; their discrepancy is about the critical density at which this occurs. A negative compressibility has a very drastic physical consequence: the system wants to get compressed without any need for an external force. Obviously such a system cannot be structurally stable; it should collapse beyond this critical density. The stability of real systems (such as metals, semiconductors) is established by the positive background [34]; recall that in the EL model we assume the positive background to be rigid, which cannot respond to any perturbation. For this reason, we can call this peculiar effect as the negative *electronic* compressibility, to spare room for the ionic contribution. The speculative nature of this subject has recently changed, by the announcement of Eisenstein and co-workers about the measurement of a negative electronic compressiblity of a 2D quantum well, which is actually a quasi-2D structure [41]. Very recently, Cambridge group also reported their results [42] on the compressibility of the quantum wells, confirming the previous experiment, but claimed to be with better accuracy. Furthermore, it is pointed out that, for the compressibility of quantum wells with large well widths, the contribution of the Hartree band bending term is sizeable. As a matter of fact, the theoretical predictions of Gold and Calmels' [43] on the compressibility of quasi-2D quantum wells ignoring this term is shown to be in large disagreement with the experimental data [42].

Negative compressibility is intimately related to the negative long-wavelength static DF. Figures 8-10 (b) indicate the negative $q-$zone of the static DF. As Dolgov *et al.* [44] have pointed, a negative static DF does not contradict with the causality, as a matter of fact, this feature is shared by most of the techniques beyond the RPA including the QMC. The physical consequence of a negative static DF is that an external impurity can be screened by more than the equal amount of opposite charge. This effect is sometimes named as *anti-screening* (see, for instance, Ref. [45]), however, here we prefer the word *overscreening*. A curious point that has not been addressed in the literature is the driving mechanism of this effect, which we recently raised in a previous work [46]. To illuminate this point, we first investigate different physical systems that show an overscreening. First of all overscreening is not limited to i) 2D ELs, it exists in 3D EL as well (see, for instance, Figure 5 (b)), moreover, ii) this effect is present also in Bose liquids [47], furthermore, iii) classical liquids show overscreening too [1]. These diverse examples reveal that overscreening is not due to a i) dimensionality effect, or to a ii) quantum statistical effect, or to a iii) quantum mechanical effect, respectively. A common feature in all these example cases is that overscreening is observed for low particle densities where the strong potential energy dominates the system behavior, which leads us to conclude that overscreening is driven by a liquid-solid transition. This subject is still premature and an important initial step is to determine the phase diagram in the density-temperature plane of the "normal" electron liquid.

9. Conclusions

The knowledge of the wave number- and frequency-dependent DF is highly rewarding, as a variety of many-body related terms such as the self-energy, carrier lifetime, and mobility are then routinely accessible [5]. For this reason an accurate dielectric characterization is vital for the equilibrium and electronic transport properties. Going beyond the RPA, we pursue a systematic assessment of the STLS DF by comparing it with QMC data and the polarization potential theory of Pines and co-workers both in 3D and 2D. Apart from the violation of the compressibility sum rule, which shows itself with a poor long-wavelength behavior, and the degraded form towards the Wigner solid densities, STLS displays an impressive performance within the practical electron densities. We can summarize our observations on the STLS DF as, a good agreement with the QMC for intermediate and small wavelengths over all realistic r_s values, and almost non-negative pair-correlation function. However, for the low-dimensional, artificial electronic structures, the most important virtue of the STLS technique, is its self-consistent scheme which does not require any fitting to experiment or simulation data (in contrast to the pseudopotential approach), where QMC data is not available. For the 2D EL we calculate the correlation energy and the compressibility and compare them with the other approaches. Dominating electron-electron interactions towards the low densities causes interesting phenomena such as the negative electronic compressibility and the overscreening of charged impurity centers.

We would like to reserve our final words to certain challenges on the DF of the EL beyond the RPA level. A major current issue is to account for the inertia of the Pauli-Coulomb hole around each electron, that is to say, replacing the static LFC with a dynamic (frequency-dependent) one. Even though several recent attempts have been made towards this direction [48, 49], this field has not become mature yet. Another possible improvement to STLS-type treatments is the inclusion of the multi-pair excitations, which was particularly stressed in Ref. [32].

References

[1] S. Ichimaru, *Rev. Mod. Phys.* **54** (1982) 1017.

[2] A. Isihara in *Solid State Physics*, ed. H. Ehrenreich, and D. Turnbull, vol. 42 (Academic, New York, 1989) p. 271.

[3] N. D. Mermin, *Phys. Rev. B* **1** (1970) 2362.

[4] A. K. Das, *J. Phys. F* **5** (1975) 2035.

[5] G. Mahan, *Many-Particle Physics*, 2nd ed. (Plenum, New York, 1990).

[6] D. Pines and P. Nozières, *The Theory of Quantum Liquids*, vol. I (Benjamin, New York, 1966).

[7] C. Bulutay and M. Tomak, *Phys. Rev. B* **54** (1996) 14643.

[8] C. Bulutay, I. Al-Hayek, and M. Tomak, in review (preprint: cond-mat/9708103).

[9] C. Bowen, G. Sugiyama, and B. J. Alder, *Phys. Rev. B* **50** (1994) 14838.

[10] L. V. Keldysh, D. A. Kirzhnitz, and A. A. Maradudin (editors), *The Dielectric Function of Condensed Systems*, (Elsevier, Amsterdam, 1989).

[11] C. Balanis, *Advanced Engineering Electromagnetics*, (Wiley, New York, 1989).

[12] H. Haug and S. Schmitt-Rink, *Prog. Quant. Electr.* **9** (1984) 3.

[13] A. L. Fetter and J. D. Walecka, *Quantum Theory of Many-Particle Systems* (McGraw-Hill, New York, 1971).

[14] J. Lindhard, *Kgl. Danske Videnskab. Selskab, Mat. Fys. Medd.* **28** (1954) No. 8.

[15] V. D. Gorobchenko, V. N. Kohn, E. G. Maksimov in *The Dielectric Function of Condensed Systems* ed. L. V. Keldysh, D. A. Kirzhnitz, and A. A. Maradudin (Elsevier, Amsterdam, 1989).

[16] K. S. Singwi, M. P. Tosi, R. H. Land, A. Sjölander, *Phys. Rev.* **176** (1968) 589.

[17] C. Bulutay, Ph. D. Thesis, Department of Electrical and Electronics Engineering, Middle East Technical University, Ankara, Turkey, 1997.

[18] D. Pines, *Elementary Excitations in Solids* (Benjamin, New York,1963).

[19] P. V. Panat and V. V. Paranjape, *Solid State Commun.* **62** (1987) 829.

[20] J. Hubbard, *Proc. R. Soc. A* **243** (1957) 336.

[21] N. Iwamoto, *Phys. Rev. B* **43** (1991) 2174.

[22] G. Barton, *Elements of Green's Functions and Propagation: potentials, diffusion and waves* (Clarendon, New York, 1989).

[23] J. S. Thakur and K. N. Pathak, *J. Phys. C* **16** (1983) 6551.

[24] D. Olego, A. Pinczuk, A. C. Gossard, and W. Wiegmann, *Phys. Rev. B* **26** (1982) 7867.

[25] F. Stern, *Phys. Rev. Lett.* **18** (1967) 546.

[26] C. Bulutay and M. Tomak, *Phys. Rev. B* **53** (1996) 7317.

[27] G. D. Mahan, *Phys. Scr.* **32** (1985) 423.

[28] L. C. Ioriatti and A. Isihara, *Z. Phys. B* **44** (1981) 1.

[29] U. de Freitas and N. Studart, *Phys. Rev. B* **36** (1987) 6677.

[30] S. Moroni, D. M. Ceperley, and G. Senatore, *Phys. Rev. Lett.* **75** (1995) 689.

[31] D. Pines, in *Highlights of the Condensed-Matter Theory*, Proceedings of the International School of Physics "Enrico Fermi ", ed. F. Bassani, F. Fumi, and M. P. Tosi (North-Holland, Amsterdam 1985) p. 580.

[32] N. Iwamoto and D. Pines, *Phys. Rev. B* **29** (1984) 3924.

[33] N. Iwamoto, E. Krotscheck, and D. Pines, *Phys. Rev. B* **29** (1984) 3936.

[34] B. Tanatar, and D. M. Ceperley, *Phys. Rev. B* **39** (1989) 5005.

[35] S. Moroni, D. M. Ceperley, and G. Senatore, *Phys. Rev. Lett.* **69** (1992) 1837.

[36] N. H. March and M. Parrinello, *Collective Effects in Solids and Liquids*, (Adam Hilger, Bristol, 1982) p. 9.

[37] D. M. Ceperley and B. J. Alder, *Phys. Rev. Lett.* **45** (1980) 566.

[38] D. J. W. Geldart and S. H. Vosko, *Can. J. Phys.* **44** (1966) 2137.

[39] G. Senatore, private communication.

[40] N. Iwamoto, *Phys. Rev. B* **30** (1984) 3289.

[41] J. P. Eisenstein, L. N. Pfeiffer, and K. W. West, *Phys. Rev. B* **50** (1994) 1760.

[42] N. K. Patel, I. S. Millard, C. Foden, E. H. Linfield, M. Y. Simmons, D. A. Ritchie, and M. Pepper, *Superlatt. Microstruc.* **21** (1997) 125 .

[43] A. Gold and L. Calmels, *Solid State Commun.* **88** (1993) 659.

[44] O. V. Dolgov, D. A. Kirzhnits, and E. G. Maksimov, *Rev. Mod. Phys.* **53** (1981) 81.

[45] K. Takayanagi, and E. Lipparini, *Phys. Rev. B* **52** (1995) 1738.

[46] C. Bulutay, N. Günalp, and M. Tomak, in *Frontiers in Nanoscale Science of Micron/Submicron Devices*, ed. A.-P. Jauho and E. V. Buzaneva, NATO ASI Series E:328, (Kluwer, Dordrecht, 1996) p. 533.

[47] G. Sugiyama, C. Bowen, and B. J. Alder, *Phys. Rev. B* **46** (1992) 13042.

[48] A. Holas and S. Rahman, *Phys. Rev. B* **35** (1987) 2720.

[49] R. K. Moudgil, P. K. Ahluwalia, and K. N. Pathak, *Phys. Rev. B* **52** (1995) 11945.